ACS Catalysis

pubs.acs.org/acscatalysis

Research Article

How Size Matters: Electronic, Cooperative, and Geometric Effect in Perovskite-Supported Copper Catalysts for CO_2 Reduction

Drejc Kopač, Blaž Likozar,* and Matej Huš*

Cite This: *ACS Catal.* 2020, 10, 4092−4102

Read Online

ACCESS | Metrics & More | Article Recommendations | Supporting Information

ABSTRACT: In heterogeneous catalysis, bifunctional catalysts often outperform one-component catalysts. The activity is also strongly influenced by the morphology, size, and distribution of catalytic particles. For CO_2 hydrogenation, the size of the active copper area on top of the $SrTiO_3$ perovskite catalyst support can affect the activity, selectivity, and stability. Here, a detailed theoretical study of the effect of bifunctionality on an important chemical CO_2 transformation reaction, the reverse water gas shift (RWGS) reaction, is presented. Using density functional theory computation results for the RWGS pathway on three surfaces, namely, Cu(111), $SrTiO_3$, and the Cu/$SrTiO_3$ interface between both solid phases, we construct the energy landscape of the reaction. The adsorbate−adsorbate lateral interactions are taken into account for catalytic surfaces, which show a sufficient intermediate coverage. The mechanism, combining all three surfaces, is used in mesoscale kinetic Monte Carlo simulations to study the turnover and yield for CO production as a function of particle size. It is shown that the reaction proceeds faster at the interface. However, including copper and the support sites in addition to the interface accelerates the conversion even further, showing that the bifunctionality of the catalyst manifests in a more complex interplay between the phases than just the interface effect, such as the hydrogen spillover. We identify three distinct effects, the electronic, cooperative, and geometric effects, and show that the surrounded smaller Cu features on the set of supporting $SrTiO_3$ show a higher CO formation rate, resulting in a decreasing RWGS model trend with the increasing Cu island size. The findings are in parallel with experiments, showing that they explain the previously observed phenomena and confirming the size sensitivity for the catalytic RWGS reaction.

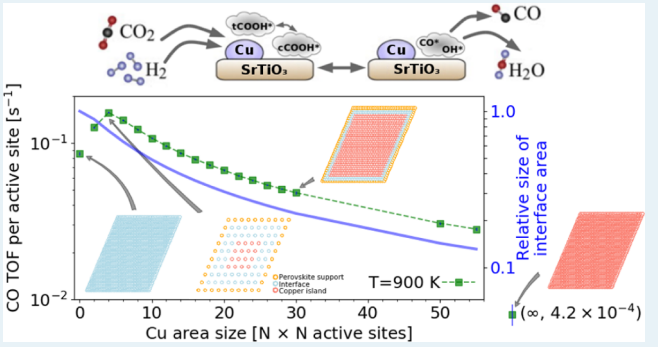

KEYWORDS: *CO_2 reduction, RWGS, copper, perovskite, bifunctional catalyst, promoter effect, first principles*

INTRODUCTION

In the field of heterogeneous catalysis, the quest for the "perfect" catalyst has been the central topic since time immemorial. Through more than a century of experiments and several decades of simulations, we have learnt that choosing the right catalytic material is only one part of the puzzle. The effectiveness of a catalyst is in large part determined by the structural and geometric parameters of the surface, such as the facet exposed, the abundance of crystallite boundaries, the aggregation (sintering) in multi-component catalysts, and so forth. Bifunctional catalysts often outperform pure catalysts, where the interface between different components is believed to play a decisive role. The amount of interface active sites is intimately connected to the dispersion of both active phases. In extreme cases, the behavior of nano-sized catalytic particles is completely different from the large-scale activity of the same material.

The effect of the size of the active region, whether in terms of metal particle size or coverage, has been extensively studied in the literature in the context of catalytic activity and selectivity.[1−5] Several studies have shown that there is a correlation between the turnover frequency (TOF, measured as the number of product molecules produced per second on an active site) and the size of the catalytically active region (structure sensitivity). It has been argued that the nanoscale metal particles alter the structure to the point such that more surface is exposed for smaller sizes, resulting in a higher concentration of active sites.[6] For instance, it has been shown that smaller PdZn particles in the Pd/ZnO catalysts lead to a higher TOF for the CO formation in the RWGS (reverse water gas shift) reaction.[7] Conversely, for methanol synthesis over Cu-type catalysts, several copper atoms increase the TOF for methanol formation, whereas smaller copper particles (below 8

Received: December 9, 2019
Revised: February 5, 2020
Published: March 5, 2020

https://dx.doi.org/10.1021/acscatal.9b05303
ACS Catal. 2020, 10, 4092−4102

nm) decrease the TOF because of the lack of step-edge defects,[6] which are shown to be more catalytically active.[8]

In this study, we focus on the RWGS reaction because of its importance in the carbon society. CO_2 can be used as a feedstock to produce fuels or bulk chemicals for the chemical industry. Also, carbon capture and utilization represents one of the mitigation processes for preventing further increases in the CO_2 concentration in the atmosphere. Catalytic CO_2 hydrogenation and conversion to carbon fuels, in particular via CO as an intermediate for the Fischer−Tropsch process, are of particular industrial importance.[9−12] Because a selective reduction of CO_2 at high temperatures via heterogeneous catalysis is an energetically expensive process, the use of optimized catalysts or an attractive alternative approach is essential.[13]

The RWGS reaction is one of the primary reactions to form CO from CO_2.[14,15] Because the RWGS reaction is an endothermic reaction, it is typically carried out at higher temperatures (up to 1000 K) and lower pressures (1 bar). However, the RWGS reaction at temperatures in the range of 500−650 K is also possible provided a suitable catalyst is used.[16,17] Catalysts for the RWGS are usually bifunctional and based on Cu or noble metals, which is also the case for methanol synthesis. At higher temperatures and lower pressures, RWGS is the dominant pathway.[18,19] On bifunctional metal−metal oxide catalysts, CO is formed primarily via the C═O bond cleavage.[20] Hydrogen spillover from the metal to the interface-support surface engages the CO_2 hydrogenation at the interface region.[21,22] Similarly, CO formation is promoted at the interface, which commonly acts as a step-edge defect, lowering the activation energy for intermediate dissociation and enhancing the catalytic activity.

In this paper, we provide a theoretical first-principles and kinetic explanation of an experimentally well-known phenomenon that the catalytic activity of bifunctional catalysts exceeds that of monometallic catalysts and is also dependent on the dispersion and/or sintering. As a model system, the RWGS reaction on a $Cu/SrTiO_3$ catalyst proved ideal. In addition to being an industrially and scientifically important reaction, there are abundant experimental data on it. Although Cu is a well-known catalyst for CO/CO_2 reactions, $SrTiO_3$ in the perovskite structure has its own useful properties. Supported perovskite oxides have been used for the low-temperature RWGS reaction, showing the potential for industrial-scale applications.[23] $SrTiO_3$ is a suitable candidate for studying RWGS also because of its tendency toward CO_2 adsorption, favoring CO_2 activation, while at the same time, CO as the final RWGS product is known to adsorb weakly on $SrTiO_3$.[24] Although experiments show that TiO_2 binds CO_2 more strongly, the reaction proceeds faster on $SrTiO_3$.[25] $SrTiO_3$ also harbors a great potential for the future. It had already been studied for photocatalysis applications because of a suitable band gap.[26] It is considered as a gold standard for catalytic wastewater treatment and solar water splitting reaction.[27] Thus, combining $SrTiO_3$ with various metals can extend its use to heterogeneous catalysis, electron transport material in solar cells, solid fuel cell electrodes, and so forth.[28−30] Copper was modeled as the Cu(111) surface, which is the most stable facet and appears most abundantly under relevant conditions.[31] Moreover, the (111) facets of face-centered cubic (fcc) metals are most often used in computational studies to investigate general observations and trends.[32−34]

We study the effect of the active site region in a bifunctional $Cu/SrTiO_3$ catalyst for the RWGS reaction. The superior activity of bifunctional catalysts is shown to be caused by three effects: the electronic effect, the cooperative effect, and the geometric effect. We first show that the interface is inherently more active than each of its constituent phases alone (electronic effect). We then show that its connection to the copper phase further increases the activity (cooperative effect). Last, we show that the size of Cu "islands" on the perovskite support is crucial for the activity (geometric effect).

We employ a first-principle-based multiscale modeling,[35] consisting of density functional theory (DFT) and kinetic Monte Carlo (kMC) calculations. DFT is used to characterize the material properties and geometry and to assess the energetics, kinetics, and thermodynamics of the RWGS reaction. Three regions, present in the bifunctional catalyst, were investigated: the copper Cu(111) surface acting as an active surface, the interface region between the Cu and $SrTiO_3$ perovskite, and the $SrTiO_3$ perovskite acting as a support material. Catalytic activity was calculated from kMC simulations. In particular, the transport of the adsorbed particles between the three regions was explicitly modeled. For a veracious description, the adsorbate−adsorbate nearest-neighbor lateral interactions are taken into account. We show that the $SrTiO_3$ support material is catalytically inactive for the RWGS reaction. The metal Cu surface is active for the dissociative adsorption of hydrogen, which spills over to the $Cu/SrTiO_3$ interface, where further reactions take place, ultimately leading to the formation of CO. The results are consistent with the existing experimental data and provide an atomistic and structural underpinning for them.

METHODS

Ab Initio DFT Calculations. We used Vienna Ab Initio Simulation (VASP) package (v 5.4.1) to perform plane-wave DFT calculations.[36−38] To describe the interaction between valence electrons and cores, projector-augmented wave pseudopotentials were used,[39,40] using the Perdew−Burke−Ernzerhof exchange−correlation functional.[41] The van der Waals interactions were taken into account via the zero damping DFT-D3 dispersion correction of Grimme.[42] Based on convergence testing, the kinetic energy cutoff of 450 eV was used. All structures were relaxed until the forces dropped below 0.01 eV/AÅ, while for the transition states, the threshold was set to 0.03 eV/AÅ. A vacuum thickness of at least 12 Å above the surface was used to prevent spurious slab interactions along the z direction. Depending on the surface, the sampling of a Monkhorst−Pack k-point grid[43] with $4 \times 4 \times 1$, $2 \times 4 \times 1$, and $2 \times 2 \times 1$ points was used for Cu(111), $SrTiO_3$, and $Cu/SrTiO_3$ surfaces, respectively, as the unit cells were of different sizes. The transition-state search was performed using the nudge elastic band method,[44−46] and the obtained saddle points were refined using the dimer method.[47−50]

The vibrational frequencies of adsorbates and transition states were obtained by calculating the Hessian matrix with a finite difference approach, using a step size of 0.02 AÅ. The obtained frequencies were used in the calculations of the partition functions, in the pre-exponential factors of the rate equations, and for the zero-point energy (ZPE) correction, calculated as

https://dx.doi.org/10.1021/acscatal.9b05303
ACS Catal. 2020, 10, 4092−4102

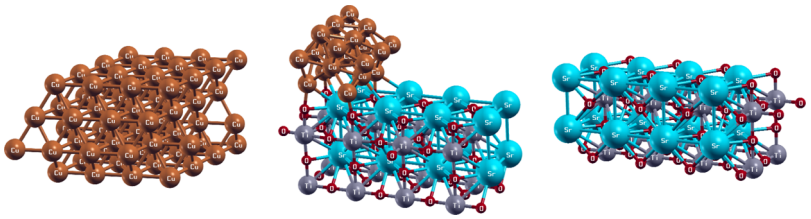

Figure 1. Three surfaces were theoretically modeled for the RWGS reaction. From left to right: Cu(111) (island surface), Cu/$SrTiO_3$ (interface surface), and $SrTiO_3$ (support surface).

$$E_{ZPE} = \frac{1}{2}hc\sum_i \nu_i \quad (1)$$

where ν_i represents the vibrational mode wavenumber (in cm^{-1}). Spin-polarized calculations have been performed on $SrTiO_3$ and Cu/$SrTiO_3$, while on Cu, magnetic moments are quenched. Dipole corrections in vacuum were used to counterbalance the errors due to periodic boundary conditions.[51,52] XCrysDen (v 1.5.6) was used for visualization and structure plots.[53]

Mesoscale kMC Simulations. We used a graph-theoretical kMC algorithm as implemented in the Zacros package (v 2.0) to perform kinetic mesoscale simulations.[54,55] The simulations included three distinct types of active sites: the copper surface (modeled as Cu(111) in DFT), the interface site on the Cu/$SrTiO_3$ surface (modeled as an infinite copper slab on $SrTiO_3$), and the perovskite surface [modeled as $SrTiO_3$(001)]. For each surface, the energies of the optimal adsorption site for each species are included (see the Supporting Information). Thus, the kMC setup uses one variety of active sites per surface type (i.e. we do not differentiate between the fcc, hexagonal close-packed (hcp), bridge and atop adsorption on Cu(111) but include the most stable variety for each adsorbate). For the sake of simplicity, the kMC lattice was modeled as a hexagonal lattice with periodic boundary conditions (neighbor−neighbor connectivity is 6). To estimate the statistical uncertainty of the simulations due to its stochastic nature, 10 kMC simulations with different initial random seeds were run for each set of parameters.

In total, four different types of reactions were considered: nonactivated (simple) adsorptions, activated (dissociative) adsorption of hydrogen, surface (Langmuir−Hinshelwood) reactions, and direct reactions of gaseous species on the surface [Eley−Rideal (E−R)]. In general, the kinetics follow the Arrhenius law

$$k = \alpha \exp\left(-\frac{E_A(\sigma)}{k_B T}\right) \quad (2)$$

where $E_A(\sigma)$ is the activation energy depending on the neighboring adsorbate configuration σ (lateral interactions influence it) and α is the pre-exponential factor calculated according to the transition-state theory (as a function of the vibrational, rotational, and translational partition functions, which in turn also depend on the temperature and in the case of adsorption pressure). Kinetic parameters are obtained from the DFT calculations, as described in the previous section. Detailed expressions for the reaction rates have already been published.[54,56−59] In general, for Langmuir−Hinshelwood surface reactions, the pre-exponential factor is of the order of $k_B T/h \approx 10^{13}$ s^{-1} for both forward and reverse reactions. For the reactions involving gaseous species (adsorption and E−R reactions), the pre-exponential factor is also strongly dependent on partial pressure, molecule size, and the reaction site area (i.e. surface density). The sticking factor was assumed to be unity for all reaction rates.[60] All simulated reactions are considered reversible. The simulations were run for 3×10^5 s, which sufficed for $\sim 10^9$ elementary steps. The reaction time progressed to $\sim 10^3$ to 10^6 s, depending on the lattice size and operating temperature, which was sufficient to reach a steady-state operation (typically after ~1 s). The system was simulated at 600 and 900 K to study low- and high-temperature laboratory conditions at pressure 1 bar with a gas molar fraction H_2/CO_2 = 3:1.

RESULTS AND DISCUSSION

First-Principles Catalyst Structure. Copper and perovskite catalysts were modeled as four-layer slabs of Cu(111) and $SrTiO_3$(001), which are the preferred and most stable surface facets.[61,62] The bottom two layers were frozen in their bulk position in the DFT simulations, while other layers and adsorbates were left free to relax. Bulk calculations yielded lattice constants of 3.63 Å for copper and 3.93 Å for $SrTiO_3$, which is consistent with experimentally determined values to within ~1%. According to our convergence testing, a 4 × 4 supercell and a 4 × 2 supercell for copper and perovskite, respectively, were sufficient for well-converged results. The complete energetics for the Cu/$SrTiO_3$ interface was obtained from our previous work.[59] All DFT parameters were consistent across the calculations on all three surfaces. There was 12, 19, and 15 Å of vacuum between the Cu(111), $SrTiO_3$(001), and Cu/$SrTiO_3$ slabs, respectively.

Cu/$SrTiO_3$ was modeled as in our previous work.[59] On a 4 × 2 supercell of $SrTiO_3$(001), which is commensurate with the copper lattice, an infinitely long copper deposition, cut along the (100) and (111) surfaces from the bulk copper structure, was placed. The reaction is modeled at the (111) surface of the copper rod. Several positions were considered to find its global minimum, which was verified by molecular dynamics. For more information, the reader is referred to our previous work.[59]

Figure 1 shows the optimized structures that were studied. Throughout the text, we assume the following notation: the catalytically active Cu(111) sites are named "islands", the Cu/$SrTiO_3$ surface active sites are termed as the interface sites, and the $SrTiO_3$ surface sites are termed as the support sites. For each species, several adsorption sites on each surface were tested (such as bridge, hcp, fcc, and atop). In each case, the optimal configuration with the lowest total energy was used for further calculations.

Reaction Pathway and Energetics. There are two main pathways for CO_2 hydrogenation: the formate pathway consisting of CO_2, HCOO, H_2COO or HCOOH, H_2COOH

https://dx.doi.org/10.1021/acscatal.9b05303
ACS Catal. 2020, 10, 4092−4102

or H_2CO, H_3CO, and CH_3OH and the RWGS pathway consisting of CO_2, t-COOH, c-COOH, CO, and, if run in methanol producing conditions, HCO, H_2CO, H_3CO, and CH_3OH. A direct dissociation of CO_2 to CO and O is unlikely on the Cu(111)[63] or the Cu/$SrTiO_3$ interface.[59] Thus, a five-step reaction mechanism was chosen for this work.

First, hydrogen molecules are activated in a dissociative adsorption step, which can occur on island or interface sites. Although the activation barrier on Cu(111) is larger than on the interface (0.26 vs 0.11 eV), hydrogen is still predominantly activated on them, as shown later on. This effect has a purely thermodynamic cause. The energy of adsorption on Cu(111) is more favorable than on interface sites (−0.64 vs −0.52 eV). More importantly, the repulsive lateral interaction between two coadsorbed H* is negligible on copper (0.04 eV) and considerable on the interface (0.30 eV). As a consequence, hydrogen is preferentially adsorbed on Cu(111). A fraction of it then spills over to the interface sites, where hydrogenation reactions occur. The perovskite itself is inactive toward hydrogen dissociation.

In the RWGS reaction, a direct cleavage of one C═O bond in CO_2 has a prohibitively large activation barrier and was omitted from the reaction pathway. As shown by Grabow and Mavrikakis,[63] this reaction has a barrier of ∼1.8 eV on Cu(111). If CO_2 cannot bind in a bent orientation (such as on Cu(111)), the barrier for its dissociation is of the order of ∼3 eV.[64] Therefore, this reaction is usually not included in the reaction networks on extended surfaces, such as Cu(111).[33,65] It has been shown, however, that on more rugged Cu surfaces, the barrier is lower.[66]

We thus follow the hydrogenation route of CO_2. As shown computationally for different copper-containing catalysts, CO forms upon the hydrogenation of CO_2 on the oxygen atom, yielding t-COOH.[63,67] Theoretically, CO_2 could also be hydrogenated on the carbon atom to yield the formate species (HCOO), but this reaction has been shown to be a mechanistic dead-end, relevant only for methanol production.[68] Our results corroborate and extend these findings. On island sites, the barrier for the formation of t-COOH was found to be 0.91 eV with respect to the gaseous reactant (1.31 eV for the adsorbed site), which agrees well with the value from Zhao et al.[68] (1.27 eV). This reaction is much more favorable on the interface, where the activation barrier drops to 0.31 eV and the reaction energy is only +0.18 eV. On the support, this reaction is prohibitively endothermic with a very large barrier (1.69 eV).

Because of geometric constraints, t-COOH cannot decompose directly. Instead, its isomerization yields c-COOH, which can then easily dissociate into CO and OH. The isomerization step can occur on all three types of sites (island, interface, and support). The reaction is almost thermoneutral and has a low activation barrier. However, as other hydrogenation reactions occur primarily at the interface, there is insufficient t-COOH for isomerization elsewhere. The dissociation of c-COOH has very low activation barriers on copper and support sites, which is consistent with the literature data.[63] However, the reaction can also happen at the interface, where the concentration of c-COOH is expected to be much higher. CO is the product of this dissociation and preferentially desorbs as opposed to be further hydrogenated.[63] The ensuing OH species further reacts with hydrogen to form water, which also desorbs.

A tabular representation of the calculated adsorption energies and activation barriers is shown in Tables 1 and 2, respectively. In Table 2, all included elementary reactions with their activation and reaction energies are summarized. As diffusion is of paramount importance when studying the interplay of different regions, special emphasis was placed on incorporating its effects. As shown in Table 2, only the diffusion of adsorbed hydrogen atoms was required. Namely, H_2 is dissociatively adsorbed and H* is then allowed to diffuse between neighboring active sites or migrate (hop) from the island site to the interface site and vice versa, allowing for the hydrogen spillover.

Table 1. Adsorption Energies (with ZPE Corrections) for the Adsorbates in the RWGS Reaction for All Three Surfaces (Labeled as in Figure 1)

	E_{ads}^{ZPE} [eV]		
adsorbate	Cu(111)	Cu/$SrTiO_3$	$SrTiO_3$
H	−0.32	−0.26	−0.04
CO_2	0.40	−0.42	−0.10
t-COOH	−1.69	−2.49	−1.02
c-COOH	−1.80	−2.37	−1.20
CO	−1.04	−1.03	−0.22
OH	−3.03	−3.57	−2.81
H_2O	−0.30	−1.03	−0.35

We rationalize the inclusion of hydrogen diffusion only, as follows. CO_2 can adsorb on all surfaces. On the other hand, it can even react via the E−R mechanism directly from the gaseous phase. Other species were found to be not mobile within the reaction time frame. Being unstable species in the bulk, their adsorption is so exothermic and their diffusion barrier is so high such that they can be considered immobile without the loss of accuracy. For instance, the barrier of the decomposition of c-COOH is ∼1 eV lower than its diffusion barrier. It was also not necessary to include the diffusion of CO and its spillover as it is the final product, which ultimately desorbs. As explained above, further hydrogenation of CO was not included based on the thermodynamic grounds for the reaction at the given conditions. In Figure 2, the potential energy diagrams for all three surfaces are shown.

Adsorbate−adsorbate interactions can play a crucial role in the ultimate performance of a catalyst, (dis)favoring reactions differently than one would expect from the potential energy diagrams. Thus, we include the lateral interactions explicitly in the model. Preliminary testing showed that truncating the cluster expansion[55] after the 1NN (first nearest-neighbor) term sufficed for reliable results. As shown by DFT calculations and kinetic modeling, respectively, the surface coverages are low enough and further terms are small enough for the assumption to be warranted. Moreover, as atomic hydrogen is the most abundant species on the surface, only pairwise interactions including H* were considered. The interaction energy was calculated as

$$E_{lateral} = E_{H^*+X^*} - E_{H^*} - E_{X^*} + E_{catalyst} \quad (3)$$

where E_{H^*} is the total energy of the system with adsorbed H*, E_{X^*} is the total energy of the system with an adsorbed intermediate X*, and $E_{H^*+X^*}$ is the total energy of the system with H* and X* coadsorbed on adjacent sites. $E_{catalyst}$ is the total energy of the empty catalyst. In Table 3, the DFT calculated pairwise interaction energies are listed. Because of the exceedingly high reaction barriers on the support sites, prohibiting hydrogenation reactions, lateral interactions did not have to be calculated for these sites.

https://dx.doi.org/10.1021/acscatal.9b05303
ACS Catal. 2020, 10, 4092−4102

Table 2. ZPE-Corrected Activation Barriers (E_A^{ZPE}) and Reaction Energies (ΔE^{ZPE}) of the Simulated Elementary Reaction Steps for the RWGS Mechanism on All Three Surfaces[a]

	Cu(111)		$Cu/SrTiO_3$		$SrTiO_3$	
reaction	E_A^{ZPE}	ΔE^{ZPE}	E_A^{ZPE}	ΔE^{ZPE}	E_A^{ZPE}	ΔE^{ZPE}
$H_2(g) \leftrightarrow H + H$	0.26	−0.64	0.11	−0.52	1.65	0.37
$CO_2 + H \leftrightarrow$ t-COOH	0.91	0.27	0.31	0.18	1.69	0.88
t-COOH ↔ c-COOH	0.31	−0.04	0.51	0.20	0.32	−0.11
c-COOH ↔ CO + OH	0.09	−0.60	0.83	−0.40	0.07	0.01
$OH + H \leftrightarrow H_2O$	1.07	0.15	0.82	−0.25	0.95	−0.78
H (Cu) ↔ H (Cu)	0.11	–	n/a	n/a	n/a	n/a
H (Cu) → H ($Cu/SrTiO_3$)	0.24	n/a	n/a	n/a	n/a	n/a
H ($Cu/SrTiO_3$) → H (Cu)	n/a	n/a	0.01	n/a	n/a	n/a
H ($Cu/SrTiO_3$) ↔ H ($Cu/SrTiO_3$)	n/a	n/a	0.30	–	n/a	n/a

[a]The lower part of the table lists the activation energies for the hydrogen diffusion and spillover (hopping) between the different active site types at the copper/interface region. All values are in eV. Surfaces labeled as in Figure 1.

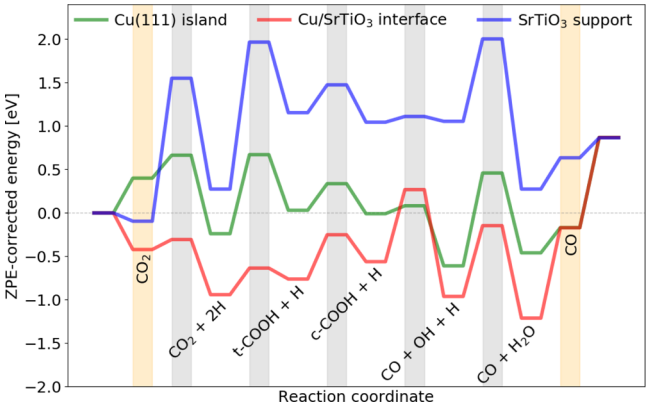

Figure 2. Potential energy surface diagram for the CO formation on all three studied surfaces. Gray shaded regions represent the transition states and orange shaded regions represent the gas adsorption/desorption steps.

Table 3. Pairwise 1NN Interactions on the Cu Island and $Cu/SrTiO_3$ Interface

	$E_{interaction}$ [eV]	
cluster configuration	Cu(111)	$Cu/SrTiO_3$
H*···H*	0.04	0.30
H*···CO*	0.10	0.09
H*···OH*	0.08	0.38
H*···H_2O*	0.04	0.05
H*···t-COOH*	0	0.17
H*···c-COOH*	0	0.12

Generally, lateral interactions at the interface sites are stronger than on island sites. This is a purely geometric effect. On Cu(111), the lattice can "reconstruct" and relax to easily accommodate two adjacent coadsorbates, while on the interface, this relaxation is much more constrained. This is consistent with the existing experimental and theoretical work. Experimentally, hydrogen−hydrogen lateral interactions are known to be small.[69] On this account, theoretical models often wholly omit lateral interactions. A complex treatment of lateral interactions on several metals by Frey et al. has shown that hydrogen adsorption energy on Cu(111) is weakly dependent on coverage.[70]

Kinetic Modeling and Size Effect. In this section, we turn our focus to the essential part of this study. With kinetic modeling (kMC), the effect of varying the size of Cu islands on the perovskite support is investigated. It is clear from geometrical considerations that upon varying the island size, the relative fraction of the interface sites changes. This has potentially large effects on the overall activity of the catalyst. Our kinetic model for the RWGS pathway consists of seven lattice adsorbates, four elementary surface reactions, and four adsorption/desorption reactions (one dissociative and three nonactivated kinetic), each for all three surfaces (islands, interface, and support).

To investigate the effect in question, the kMC simulations were carried out on differently sized lattices. Namely, we vary the dimensions of the copper islands, which results in a change in the size of the interface sites, as well. We fixed the width of the interface area to two active sites, which is according to the DFT data, a reasonable approximation. The width of the support (perovskite) was kept at one active site, as shown in Figure 3, because no catalytic activity was observed there in the preliminary testing. This assumption does not impact the results as the lattice is considered periodic and the TOFs are normalized to the number of active sites. The island sizes vary between 2 × 2 and 55 × 55. A 50 × 50 Cu(111) lattice without the interface and support was used as a benchmark to simulate infinitely large islands (or a pure Cu surface), and similarly, a hypothetical 50 × 50 lattice with only interface sites was used to simulate a catalyst where copper island sites would be catalytically inactive.

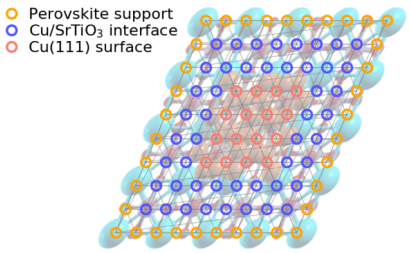

Figure 3. Lattice example for 4 × 4 Cu islands on top of the $SrTiO_3$ perovskite support. The interface region width was fixed to two active sites. The support region was confirmed to be catalytically nonactive and its width was fixed to one active site.

We first tested whether the bifunctional catalysts are in fact more active (i.e., having a higher TOF) than the monofunctional catalysts. At 500 K, a catalyst with only support (perovskite) and island (Cu) sites, lacking the interface, has a TOF of 2×10^{-8} s^{-1}. A (physically meaningless) catalyst with

https://dx.doi.org/10.1021/acscatal.9b05303
ACS Catal. 2020, 10, 4092−4102

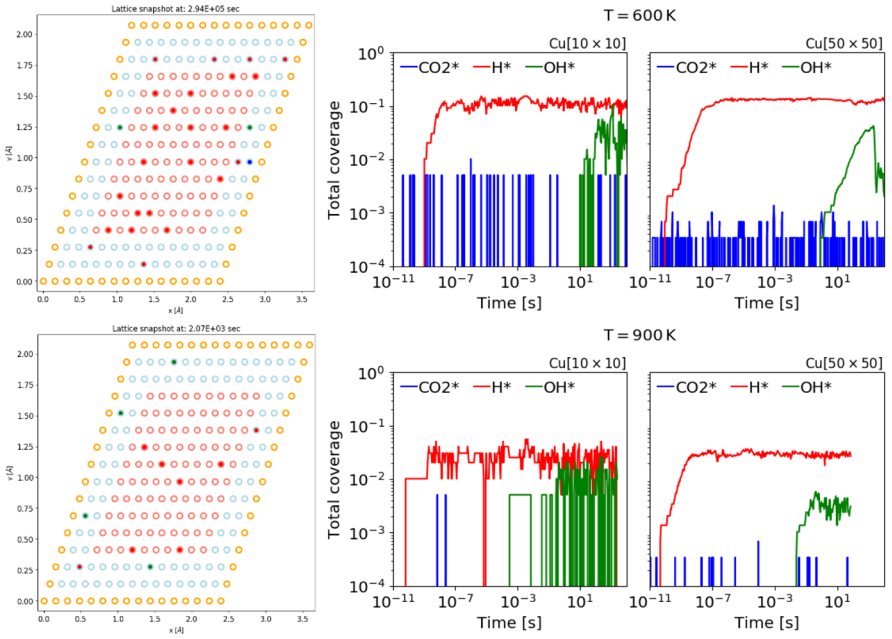

Figure 4. Lattice snapshot for a 10 × 10 Cu island (left) and the temporal evolution of the lattice coverage for 10 × 10 and 50 × 50 islands (right), all for T = 600 K (top) and T = 900 K (bottom). The most abundant lattice species is hydrogen, and the coverage is in most cases below 10%. The coverage is normalized to the number of active sites.

only interface sites and support sites has a TOF of 6.5 × 10^{-5} s^{-1}. As the electronic density at the interface region is different, we call this effect the electronic effect. In both cases, the support proved inert. A catalyst with all three types of sites (with an island size of 10 × 10) outperformed both cases with a TOF of 1.1 × 10^{-4} s^{-1}. Because this additional speed-up occurs when the interface and Cu sites are present, we call this effect the cooperative effect. In these cases, the trends are more important than absolute values. Nevertheless, experimental TOFs for CO_2 hydrogenation on copper also range from 10^{-4} to 10^{-2} s^{-1}.[71]

The simulations showed that the steady state is reached at a time scale on the order of seconds (varies slightly with the system size). In the steady state, the surface coverage of the island and interface sites is low, typically below 10% (see Figure 4), which is consistent with the microkinetic models of CO_2 activation on copper.[63] The most abundant intermediate is H*, followed by an order of magnitude lower concentration of OH*, as also observed by Grabow and Mavrikakis.[63] At a higher temperature (T = 900 K), the surface coverage is lower based on thermodynamic grounds. As every adsorption is an exothermic event, higher temperature favors desorption. Moreover, at higher temperatures, the reactions proceed faster, quickly consuming any surface intermediates. Consequently, the E−R mechanism becomes more important.

The reason why a bifunctional catalyst is more active can be explained by analyzing the reaction steps occurring on each of the active surfaces. In Figure 5, the reaction frequencies per different types of active sites (copper island or interface) are shown. The results clearly show that hydrogen is by an order of magnitude more likely to be dissociatively adsorbed on the copper islands than at the interface region. Experimentally, the importance of copper for the hydrogen activation has been noted many times.[22,72,73]

However, Cu(111) alone cannot function as an efficient catalyst for CO_2 activation. Although theoretically often researched because of the simplicity of the model, which

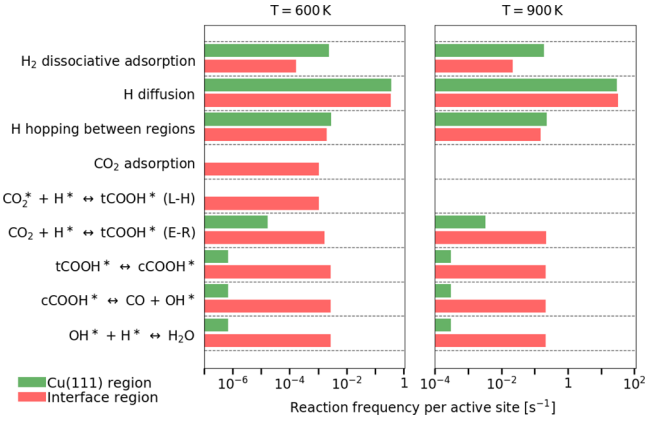

Figure 5. Step frequency histograms for 600 K (left) and 900 K (right), using a 10 × 10 Cu island. Hydrogen adsorption is faster on the Cu island, spillover (hopping) occurs to deliver hydrogen to the interface sites, where CO_2 activation takes place at a higher rate. CO_2 activation dominantly occurs via the E−R-type mechanism.

allows for an easy determination of the effect of conditions and modifications (dopants and defects),[32,74−76] experimental data unequivocally show that combined catalysts are required for practical operation.[34] Our model manages to capture this effect and explain it. Namely, CO_2 activation is faster at the interface region for almost 2 orders of magnitude. Moreover, the dominant CO_2 hydrogenation mechanism is of the E−R type. At lower temperatures, small amounts of CO_2 also react via the Langmuir−Hinshelwood route.

Also, a high frequency of hydrogen diffusion, both intra- and interphase, is discovered. This is the microscopic picture of the hydrogen spillover in action.[77] Although hydrogen is present at both phases due to the spillover, CO_2 is hydrogenated predominantly at the interface. The majority of CO is therefore produced at the interface, confirming that the perovskite support markedly improves the catalytic activity

https://dx.doi.org/10.1021/acscatal.9b05303
ACS Catal. 2020, 10, 4092−4102

for the RWGS mechanism. The support sites, although explicitly included into modeling, were devoid of any activity. Only some adsorption and desorption reactions of CO_2 and H_2 occurred at the support with negligible equilibrium coverage, not being able to sustain any spillover. The CO hydrogenation activation barrier is very high for subsequent reactions on the support.

Last, we turn our attention the effect of the island size. Changing the island size also changes the amount of interface sites, as shown in Figure 3. This changes the ratio between the island and the interface sites on the catalyst. For the island size of 10 × 10, this ratio is ∼1 and quickly increases as the islands get larger. In Figure 6, we plot the TOF versus the size of the

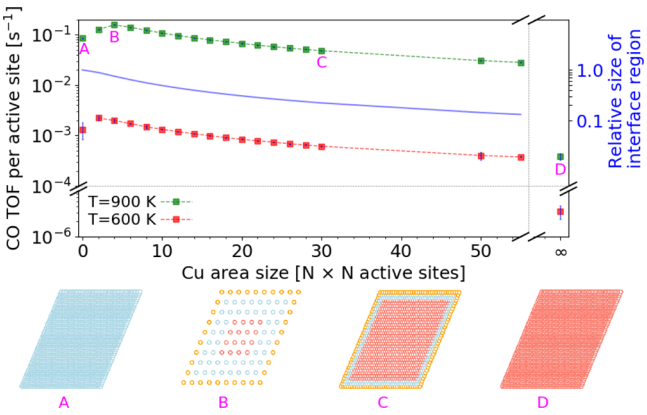

Figure 6. CO TOF as a function of the size of the Cu island. Lattice images below correspond to the marked points in the plot (A−D), representing the lattices with 0 × 0 (hypothetical surface with only interface sites), 4 × 4, 30 × 30, and apparently infinite Cu island sizes (from left to right). The green (red) points show the TOF at T = 900 K (T = 600 K). The fraction of the interface sites to all sites is plotted with a blue solid line, with y axis on the right hand side, scaled to match the CO TOF span on the left hand size.

island at two different temperatures. Expectedly, TOF is larger at higher temperatures. More important is the size effect, where a clear trend is shown. Out of scale, the TOF for an infinitely large island is also shown. There, the effect of the support, which is required for the formation of the interface, is apparent because the TOF is 3 orders of magnitude smaller than on the bifunctional catalyst.

As the island size decreases, the TOF monotonically increases. This is a consequence of a larger fraction of interface sites. Only at the smallest size at the higher temperature (900 K), the TOF drops as a very small Cu surface cannot provide enough dissociated hydrogen for the quick reaction (the effect is absent at 600 K). As discussed before, the TOF is also smaller for a hypothetical interface-only lattice, where the Cu island size is zero. There is no specific trend in the mechanism behavior as the island size varies, hinting at the fact that the size dependence of TOF is predominantly a geometric phenomenon. This is further corroborated in Figure 6, where the fraction of interface sites is plotted on the secondary axis. The TOFs follow the same trend.

The error bars in Figure 6 show the standard deviation (1σ) from the median value of all TOFs obtained at the same island size, at different initial random seeds for each kMC run. Statistically, there are no large discrepancies from the median value for most of the island sizes. Except for hypothetical surface with only interface sites and for an island size of 50 × 50 at T = 600 K, the 1σ error bars are significant, but this is purely a statistical outcome because of the discrepancies in the simulation end times for these particular cases.

Experimental Perspectives. Several studies on methanol synthesis and the RWGS reaction have linked the catalytic activity with the structure sensitivity and catalyst particle size on different catalytic materials. A study of the effect of PdZn crystallite particle size for the RWGS reaction at temperatures between 250 and 400 °C showed that smaller PdZn particles result in higher CO formation rates.[7] The RWGS reaction studied on the Pt/TiO_2 catalyst also showed that the catalytic activity was dependent on the crystallite size of the TiO_2 support but not on the structure of the Pt catalyst. As the crystallite size of TiO_2 increased, the reaction rate decreased.[78] Similarly, the rate of CO production for the RWGS reaction is higher for Cu-/ZnO-type catalysts with higher Cu dispersion, that is, smaller Cu nanoparticles are more active.[79] The RWGS reaction has also been studied on Ni/SiO_2 catalysts, where it has been shown that lower Ni loading and smaller Ni particles lead to a higher catalytic activity for the CO formation.[80] CO yields were also higher on Ru/Al_2O_3, when Ru was highly dispersed.[81]

Our results are consistent with these experimental trends, barring some caveats that stem from fundamental differences between any theoretical first-principles model and experiments. For instance, it has been shown that on Cu−ZnO and CuO−ZnO/Al_2O_3 catalysts, the total activity for the RWGS increases with an increase in the total Cu metal surface area.[82] This increase in the activity comes from the total amount of metallic sites, while in this study, the activity is normalized to the amount of metallic sites. In experiments, catalyst particles cannot be arbitrarily small. For Cu particles smaller than ∼4 nm, the rate of CO production is 3 times smaller than for larger particles (∼10 nm).[83]

Different effects are important in an experimental setup, which cannot be simply reproduced in first-principles models. The structure of the synthesized catalyst varies in particle dispersion on the support, porosity, and so forth. Different preparation methods and varied precursors result in catalysts of different surface morphologies. For instance, it has been shown that Cu/ZnO catalysts derived from the aurichalcite precursors with lower Cu content form homogeneously distributed CuO particles on the ZnO support, leading to a higher CO formation rate. This links the catalytic activity with the interface composition, brought about by the precursor and its thermal post-treatment.[84]

Catalyst structure sensitivity has also been studied thoroughly for methanol synthesis, which is a related CO_2 activation reaction. Ultrafine particles on a deposition−precipitation-prepared CuO/ZrO_2 catalyst exhibit a higher catalytic activity with a similar activity versus size trend as for the RWGS reaction.[85] On the contrary, for $Cu(Zn)/SiO_2$ and Cu/ZnO catalysts, a structure-sensitivity study showed that for Cu particles smaller than 10 nm, the activity decreases arguably because of the fact that very small particles lack a sufficient area of step-edge sites.[6,83] Another study showed that although the methanol formation rate was independent of the Cu particle size (below ∼40 nm) on Cu/ZnO catalysts, a very high Cu loading, leading to a very large Cu cluster (200 nm), can in fact cause a higher activity. This is again a consequence of the total amount of metallic sites. On $Cu/ZnO/Al_2O_3$ commercial catalysts, it has been shown that a large dispersion of Zn sites

https://dx.doi.org/10.1021/acscatal.9b05303
ACS Catal. 2020, 10, 4092−4102

on top of the Cu surface (smaller particles) results in an increased rate of methanol production.[34]

CONCLUSIONS

In this work, we have explained the synergies in a bifunctional catalyst for CO_2 hydrogenation. We took the RWGS reaction as a model reaction for CO_2 hydrogenation and a copper/perovskite substrate ($Cu/SrTiO_3$) as a model catalyst. Metal-alloyed supported perovskites are prospective candidates for low-temperature industrial catalytic processes, including RWGS. To shed light on the processes on this catalyst, we conducted DFT calculations to construct a pathway of elementary reactions leading to CO. Adsorption energies for all intermediates and reaction barriers for their interconversion were explicitly calculated for three different catalytic surfaces: a Cu(111) facet, a $Cu/SrTiO_3$ interface region, and a $SrTiO_3(001)$ perovskite surface. The kMC lattice included three types of active sites: the Cu island, the $Cu/SrTiO_3$ interface, and the $SrTiO_3$ support with separate energetics and kinetics for each of them. Lateral interactions were taken into account. We studied the catalytic activity in terms of the TOF of CO using mesoscale kMC simulations.

We present two main findings. First, the existence of the interface region itself has a favorable effect on the rate of the reaction. Artificially limiting the reaction to the interface results in higher reaction rate than on copper and perovskite sites. This effect is already used heavily in the industry, where bifunctional catalysts are the most common type of catalysts. However, allowing the reaction to proceed on all three types of sites concomitantly and enable the transfer of species across the phases via diffusion yielded an even higher reaction rate. The analysis of the relative frequencies of individual reaction steps on each surface showed that copper acts as a hydrogen source, providing sufficient amounts of atomic hydrogen that spills over to the interface. There, further hydrogenation reactions occur. No reactions occurred on the support.

Second, the size of the copper islands (a measure of sintering) has a strong effect on the reaction rate. Stemming mainly from the geometric effects, smaller copper islands result in a larger fraction of the interface sites. The increase in the reaction rate follows this relation. We varied the size area of the Cu island, which enabled us to study the TOF dependency. We show that smaller Cu islands lead to higher CO rate, with a decaying trend at larger Cu islands, explaining various similar experimental results from the literature. At T = 900 K, the TOF is 1.6×10^{-1} s^{-1} at a Cu island size 4 × 4, dropping to 2.7×10^{-2} at a Cu island size 55 × 55, and ultimately resulting in 4.2×10^{-4} s^{-1} when using only copper as a catalyst (apparently infinite size limit). A similar trend was observed at T = 600 K.

Experimental results, although mostly supporting the notion that smaller particles catalyze reaction better, are more complex than any first-principles model can predict. These trends also do not always hold at extremely small sizes. For many reactions and catalysts, it has been shown that defects, steps, kinks, and other deviations from a flat surface catalyze reactions much better than a (111) surface. Small particles can accommodate only a small number of such motifs. Second, it is important that the results are reported in a uniform fashion. Theoretically, they are usually normalized to the number of active sites. Experimental results often show a positive correlation between the amount of metallic copper and catalytic activity. Thus, such samples appear more active because of the total amount of active sites despite copper deposits being larger.

In this work, we have explained the promoting effect of the bifunctional catalysts in terms of its three constituent components. The increase in TOF is decomposed into the electronic effect, the cooperative effect, and the geometric effect. The electronic effect stems from the change in the electronic density at the interface in comparison with pure Cu(111) and $SrTiO_3(100)$. The reaction is faster on the interface sites than on the copper or support sites (combined). The cooperative effect is evidenced by an additional increase of the reaction rate when copper sites are added to the interface sites. Although the reaction is slower on pure Cu(111), having them adjoining to the interface sites increases the reaction rate further. The last effect is purely geometric—smaller copper islands have a larger interface/copper ratio. As a larger proportion of the sites is the interface sites, which are more active per se, the reaction rate is higher. This offers unique insights into the RWGS reaction on bifunctional copper/perovskite catalysts.

ASSOCIATED CONTENT

Supporting Information

The Supporting Information is available free of charge at https://pubs.acs.org/doi/10.1021/acscatal.9b05303.

DFT-relaxed geometries of stable intermediates for all three surfaces and geometries of nearest-neighbor interactions where applicable and vibrational frequencies for the intermediates and transition states, which are used for calculating vibrational partition functions and ZPE correction (PDF)

AUTHOR INFORMATION

Corresponding Authors

Blaž Likozar − *Department of Catalysis and Chemical Reaction Engineering, National Institute of Chemistry SI-1001 Ljubljana, Slovenia;* orcid.org/0000-0001-9194-6595; Email: blaz.likozar@ki.si

Matej Huš − *Department of Catalysis and Chemical Reaction Engineering, National Institute of Chemistry SI-1001 Ljubljana, Slovenia;* orcid.org/0000-0002-8318-5121; Email: matej.hus@ki.si

Author

Drejc Kopač − *Department of Catalysis and Chemical Reaction Engineering, National Institute of Chemistry SI-1001 Ljubljana, Slovenia;* orcid.org/0000-0001-8099-230X

Complete contact information is available at: https://pubs.acs.org/10.1021/acscatal.9b05303

Notes

The authors declare no competing financial interest.

ACKNOWLEDGMENTS

We acknowledge the funding from the EU Framework Programme for Research and Innovation Horizon 2020 under grant agreement no. 727504 (FReSMe) and the Slovenian Research Agency (ARRS) through Core grant P2-0152 and Project J2-7319.

https://dx.doi.org/10.1021/acscatal.9b05303
ACS Catal. 2020, 10, 4092−4102

REFERENCES

(1) Van Santen, R. A. Complementary Structure Sensitive and Insensitive Catalytic Relationships. *Acc. Chem. Res.* **2009**, *42*, 57−66.
(2) Posada-Pérez, S.; Gutiérrez, R. A.; Zuo, Z.; Ramírez, P. J.; Viñes, F.; Liu, P.; Illas, F.; Rodriguez, J. A. Highly active Au/δ-MoC and Au/β-Mo2C catalysts for the low-temperature water gas shift reaction: effects of the carbide metal/carbon ratio on the catalyst performance. *Catal. Sci. Technol.* **2017**, *7*, 5332−5342.
(3) Zhang, X.; Liu, J.-X.; Zijlstra, B.; Filot, I. A. W.; Zhou, Z.; Sun, S.; Hensen, E. J. M. Optimum Cu nanoparticle catalysts for CO2 hydrogenation towards methanol. *Nano Energy* **2018**, *43*, 200−209.
(4) Tao, H.; Li, Y.; Cai, X.; Zhou, H.; Li, Y.; Lin, W.; Huang, S.; Ding, K.; Chen, W.; Zhang, Y. What Is the Best Size of Subnanometer Copper Clusters for CO2 Conversion to Methanol at Cu/TiO2 Interfaces? A Density Functional Theory Study. *J. Phys. Chem. C* **2019**, *123*, 24118−24132.
(5) Prats, H.; Posada-Pérez, S.; Rodriguez, J. A.; Sayós, R.; Illas, F. Kinetic Monte Carlo Simulations Unveil Synergic Effects at Work on Bifunctional Catalysts. *ACS Catal.* **2019**, *9*, 9117−9126.
(6) van den Berg, R.; Prieto, G.; Korpershoek, G.; van der Wal, L. I.; van Bunningen, A. J.; Lægsgaard-Jørgensen, S.; de Jongh, P. E.; de Jong, K. P. Structure Sensitivity of Cu and CuZn Catalysts Relevant to Industrial Methanol Synthesis. *Nat. Commun.* **2016**, *7*, 13057.
(7) Lebarbier, V.; Dagle, R.; Datye, A.; Wang, Y. The effect of PdZn particle size on reverse-water-gas-shift reaction. *Appl. Catal., A* **2010**, *379*, 3−6.
(8) Kopač, D.; Likozar, B.; Huš, M. Catalysis of material surface defects: Multiscale modeling of methanol synthesis by CO2 reduction on copper. *Appl. Surf. Sci.* **2019**, *497*, 143783.
(9) Wang, W.; Wang, S.; Ma, X.; Gong, J. Recent advances in catalytic hydrogenation of carbon dioxide. *Chem. Soc. Rev.* **2011**, *40*, 3703−3727.
(10) Daza, Y. A.; Kuhn, J. N. CO2 conversion by reverse water gas shift catalysis: comparison of catalysts, mechanisms and their consequences for CO2 conversion to liquid fuels. *RSC Adv.* **2016**, *6*, 49675−49691.
(11) Porosoff, M. D.; Yan, B.; Chen, J. G. Catalytic reduction of CO2 by H2 for synthesis of CO, methanol and hydrocarbons: challenges and opportunities. *Energy Environ. Sci.* **2016**, *9*, 62−73.
(12) Liu, M.; Yi, Y.; Wang, L.; Guo, H.; Bogaerts, A. Hydrogenation of Carbon Dioxide to Value-Added Chemicals by Heterogeneous Catalysis and Plasma Catalysis. *Catalysts* **2019**, *9*, 275.
(13) Ross, M. B.; De Luna, P.; Li, Y.; Dinh, C.-T.; Kim, D.; Yang, P.; Sargent, E. H. Designing materials for electrochemical carbon dioxide recycling. *Nat. Catal.* **2019**, *2*, 648−658.
(14) Roy, S.; Cherevotan, A.; Peter, S. C. Thermochemical CO2 Hydrogenation to Single Carbon Products: Scientific and Technological Challenges. *ACS Energy Lett.* **2018**, *3*, 1938−1966.
(15) Li, W.; Wang, H.; Jiang, X.; Zhu, J.; Liu, Z.; Guo, X.; Song, C. A short review of recent advances in CO2 hydrogenation to hydrocarbons over heterogeneous catalysts. *RSC Adv.* **2018**, *8*, 7651−7669.
(16) Centi, G.; Quadrelli, E. A.; Perathoner, S. Catalysis for CO2 conversion: a key technology for rapid introduction of renewable energy in the value chain of chemical industries. *Energy Environ. Sci.* **2013**, *6*, 1711−1731.
(17) Pastor-Pérez, L.; Baibars, F.; Le Sache, E.; Arellano-García, H.; Gu, S.; Reina, T. R. CO2 valorisation via Reverse Water-Gas Shift reaction using advanced Cs doped Fe-Cu/Al2O3 catalysts. *J. CO_2 Util.* **2017**, *21*, 423−428.
(18) Bukhtiyarova, M.; Lunkenbein, T.; Kähler, K.; Schlögl, R. Methanol Synthesis from Industrial CO2 Sources: A Contribution to Chemical Energy Conversion. *Catal. Lett.* **2017**, *147*, 416−427.
(19) Liao, F.; Wu, X.-P.; Zheng, J.; Li, M. M.-J.; Kroner, A.; Zeng, Z.; Hong, X.; Yuan, Y.; Gong, X.-Q.; Tsang, S. C. E. A promising low pressure methanol synthesis route from CO2 hydrogenation over Pd@Zn core-shell catalysts. *Green Chem.* **2017**, *19*, 270−280.
(20) Kattel, S.; Liu, P.; Chen, J. G. Tuning Selectivity of CO2 Hydrogenation Reactions at the Metal/Oxide Interface. *J. Am. Chem. Soc.* **2017**, *139*, 9739−9754.
(21) Choi, S.; Sang, B.-I.; Hong, J.; Yoon, K. J.; Son, J.-W.; Lee, J.-H.; Kim, B.-K.; Kim, H. Catalytic behavior of metal catalysts in high-temperature RWGS reaction: In-situ FT-IR experiments and first-principles calculations. *Sci. Rep.* **2017**, *7*, 41207.
(22) Hu, B.; Yin, Y.; Liu, G.; Chen, S.; Hong, X.; Tsang, S. C. E. Hydrogen spillover enabled active Cu sites for methanol synthesis from CO2 hydrogenation over Pd doped CuZn catalysts. *J. Catal.* **2018**, *359*, 17−26.
(23) Hare, B. J.; Maiti, D.; Ramani, S.; Ramos, A. E.; Bhethanabotla, V. R.; Kuhn, J. N. Thermochemical conversion of carbon dioxide by reverse water-gas shift chemical looping using supported perovskite oxides. *Catal. Today* **2019**, *323*, 225−232. , Special Issue Honoring Umit S. Ozkan: 2017 ACS Henry H. Storch Award Winner
(24) Jiang-Ni, Y.; Zhi-Yong, Z.; Fu-Chun, Z. Adsorption and Reaction of CO on (100) Surface of SrTiO3 by Density Function Theory Calculation. *Chin. Phys. Lett.* **2008**, *25*, 3364−3367.
(25) Azad, S.; Engelhard, M. H.; Wang, L.-Q. Adsorption and Reaction of CO and CO2 on Oxidized and Reduced SrTiO3(100) Surfaces. *J. Phys. Chem. B* **2005**, *109*, 10327−10331.
(26) Hwang, J.; Rao, R. R.; Giordano, L.; Katayama, Y.; Yu, Y.; Shao-Horn, Y. Perovskites in catalysis and electrocatalysis. *Science* **2017**, *358*, 751−756.
(27) Lyu, H.; Hisatomi, T.; Goto, Y.; Yoshida, M.; Higashi, T.; Katayama, M.; Takata, T.; Minegishi, T.; Nishiyama, H.; Yamada, T.; Sakata, Y.; Asakura, K.; Domen, K. An Al-doped SrTiO3 photocatalyst maintaining sunlight-driven overall water splitting activity for over 1000 h of constant illumination. *Chem. Sci.* **2019**, *10*, 3196−3201.
(28) Bera, A.; Wu, K.; Sheikh, A.; Alarousu, E.; Mohammed, O. F.; Wu, T. Perovskite Oxide SrTiO3 as an Efficient Electron Transporter for Hybrid Perovskite Solar Cells. *J. Phys. Chem. C* **2014**, *118*, 28494−28501.
(29) Bi, Y.; Ehsan, M. F.; Huang, Y.; Jin, J.; He, T. Synthesis of Cr-doped SrTiO3 photocatalyst and its application in visible-light-driven transformation of CO2 into CH4. *J. CO2 Util.* **2015**, *12*, 43−48.
(30) Maiti, D.; Hare, B. J.; Daza, Y. A.; Ramos, A. E.; Kuhn, J. N.; Bhethanabotla, V. R. Earth abundant perovskite oxides for low temperature CO2 conversion. *Energy Environ. Sci.* **2018**, *11*, 648−659.
(31) Duan, X.; Warschkow, O.; Soon, A.; Delley, B.; Stampfl, C. Density functional study of oxygen on Cu(100) and Cu(110) surfaces. *Phys. Rev. B: Condens. Matter Mater. Phys.* **2010**, *81*, 075430.
(32) Yang, Y.; Evans, J.; Rodriguez, J. A.; White, M. G.; Liu, P. Fundamental studies of methanol synthesis from CO2 hydrogenation on Cu(111), Cu clusters, and Cu/ZnO(000). *Phys. Chem. Chem. Phys.* **2010**, *12*, 9909−9917.
(33) Yang, Y.; White, M. G.; Liu, P. Theoretical Study of Methanol Synthesis from CO2 Hydrogenation on Metal-Doped Cu(111) Surfaces. *J. Phys. Chem. C* **2012**, *116*, 248−256.
(34) Kattel, S.; Ramírez, P. J.; Chen, J. G.; Rodriguez, J. A.; Liu, P. Active sites for CO2 hydrogenation to methanol on Cu/ZnO catalysts. *Science* **2017**, *355*, 1296−1299.
(35) Bruix, A.; Margraf, J. T.; Andersen, M.; Reuter, K. First-principles-based multiscale modelling of heterogeneous catalysis. *Nat. Catal.* **2019**, *2*, 659−670.
(36) Kresse, G.; Hafner, J. Ab initio molecular dynamics for liquid metals. *Phys. Rev. B: Condens. Matter Mater. Phys.* **1993**, *47*, 558−561.
(37) Kresse, G.; Hafner, J. Ab initio molecular-dynamics simulation of the liquid-metal−amorphous-semiconductor transition in germanium. *Phys. Rev. B: Condens. Matter Mater. Phys.* **1994**, *49*, 14251−14269.
(38) Kresse, G.; Furthmüller, J. Efficiency of ab-initio total energy calculations for metals and semiconductors using a plane-wave basis set. *Comput. Mater. Sci.* **1996**, *6*, 15−50.
(39) Blöchl, P. E. Projector augmented-wave method. *Phys. Rev. B: Condens. Matter Mater. Phys.* **1994**, *50*, 17953−17979.
(40) Kresse, G.; Joubert, D. From ultrasoft pseudopotentials to the projector augmented-wave method. *Phys. Rev. B: Condens. Matter Mater. Phys.* **1999**, *59*, 1758−1775.

https://dx.doi.org/10.1021/acscatal.9b05303
ACS Catal. 2020, 10, 4092−4102

(41) Perdew, J. P.; Burke, K.; Ernzerhof, M. Generalized Gradient Approximation Made Simple. *Phys. Rev. Lett.* **1996**, *77*, 3865−3868.
(42) Grimme, S.; Antony, J.; Ehrlich, S.; Krieg, H. A consistent and accurate ab initio parametrization of density functional dispersion correction (DFT-D) for the 94 elements H-Pu. *J. Chem. Phys.* **2010**, *132*, 154104.
(43) Monkhorst, H. J.; Pack, J. D. Special points for Brillouin-zone integrations. *Phys. Rev. B: Solid State* **1976**, *13*, 5188−5192.
(44) Mills, G.; Jónsson, H.; Schenter, G. K. Reversible work transition state theory: application to dissociative adsorption of hydrogen. *Surf. Sci.* **1995**, *324*, 305−337.
(45) Henkelman, G.; Uberuaga, B. P.; Jónsson, H. A climbing image nudged elastic band method for finding saddle points and minimum energy paths. *J. Chem. Phys.* **2000**, *113*, 9901−9904.
(46) Henkelman, G.; Jónsson, H. Improved tangent estimate in the nudged elastic band method for finding minimum energy paths and saddle points. *J. Chem. Phys.* **2000**, *113*, 9978−9985.
(47) Henkelman, G.; Jónsson, H. A dimer method for finding saddle points on high dimensional potential surfaces using only first derivatives. *J. Chem. Phys.* **1999**, *111*, 7010−7022.
(48) Heyden, A.; Bell, A. T.; Keil, F. J. Efficient methods for finding transition states in chemical reactions: Comparison of improved dimer method and partitioned rational function optimization method. *J. Chem. Phys.* **2005**, *123*, 224101.
(49) Kästner, J.; Sherwood, P. Superlinearly converging dimer method for transition state search. *J. Chem. Phys.* **2008**, *128*, 014106.
(50) Xiao, P.; Sheppard, D.; Rogal, J.; Henkelman, G. Solid-state dimer method for calculating solid-solid phase transitions. *J. Chem. Phys.* **2014**, *140*, 174104.
(51) Neugebauer, J.; Scheffler, M. Adsorbate-substrate and adsorbate-adsorbate interactions of Na and K adlayers on Al(111). *Phys. Rev. B: Condens. Matter Mater. Phys.* **1992**, *46*, 16067−16080.
(52) Makov, G.; Payne, M. C. Periodic boundary conditions inab initio calculations. *Phys. Rev. B: Condens. Matter Mater. Phys.* **1995**, *51*, 4014−4022.
(53) Kokalj, A. XCrySDen−a new program for displaying crystalline structures and electron densities. *J. Mol. Graphics Modell.* **1999**, *17*, 176−179.
(54) Stamatakis, M.; Vlachos, D. G. A graph-theoretical kinetic Monte Carlo framework for on-lattice chemical kinetics. *J. Chem. Phys.* **2011**, *134*, 214115.
(55) Nielsen, J.; d'Avezac, M.; Hetherington, J.; Stamatakis, M. Parallel kinetic Monte Carlo simulation framework incorporating accurate models of adsorbate lateral interactions. *J. Chem. Phys.* **2013**, *139*, 224706.
(56) Pineda, M.; Stamatakis, M. Beyond mean-field approximations for accurate and computationally efficient models of on-lattice chemical kinetics. *J. Chem. Phys.* **2017**, *147*, 024105.
(57) Kopač, D.; Huš, M.; Ogrizek, M.; Likozar, B. Kinetic Monte Carlo Simulations of Methanol Synthesis from Carbon Dioxide and Hydrogen on Cu(111) Catalysts: Statistical Uncertainty Study. *J. Phys. Chem. C* **2017**, *121*, 17941−17949.
(58) Huš, M.; Kopač, D.; Štefančič, N. S.; Jurković, D. L.; Dasireddy, V. D. B. C.; Likozar, B. Unravelling the mechanisms of CO2 hydrogenation to methanol on Cu-based catalysts using first-principles multiscale modelling and experiments. *Catal. Sci. Technol.* **2017**, *7*, 5900−5913.
(59) Huš, M.; Kopač, D.; Likozar, B. Catalytic Hydrogenation of Carbon Dioxide to Methanol: Synergistic Effect of Bifunctional Cu/Perovskite Catalysts. *ACS Catal.* **2019**, *9*, 105−116.
(60) Prats, H.; Álvarez, L.; Illas, F.; Sayós, R. Kinetic Monte Carlo simulations of the water gas shift reaction on Cu(111) from density functional theory based calculations. *J. Catal.* **2016**, *333*, 217−226.
(61) Liborio, L. M.; Sánchez, C. G.; Paxton, A. T.; Finnis, M. W. Stability of Sr adatom model structures for SrTiO3(001) surface reconstructions. *J. Phys.: Condens. Matter* **2005**, *17*, L223−L230.
(62) Heifets, E.; Piskunov, S.; Kotomin, E. A.; Zhukovskii, Y. F.; Ellis, D. E. Electronic structure and thermodynamic stability of double-layered $SrTiO_3$(001) surfaces: Ab initio simulations. *Phys. Rev. B: Condens. Matter Mater. Phys.* **2007**, *75*, 115417.
(63) Grabow, L. C.; Mavrikakis, M. Mechanism of Methanol Synthesis on Cu through CO2 and CO Hydrogenation. *ACS Catal.* **2011**, *1*, 365−384.
(64) Hagman, B.; Posada-Borbón, A.; Schaefer, A.; Shipilin, M.; Zhang, C.; Merte, L. R.; Hellman, A.; Lundgren, E.; Grönbeck, H.; Gustafson, J. Steps Control the Dissociation of CO2 on Cu(100). *J. Am. Chem. Soc.* **2018**, *140*, 12974−12979.
(65) Maulana, A. L.; Putra, R. I. D.; Saputro, A. G.; Agusta, M. K.; Nugraha, N.; Dipojono, H. K. DFT and microkinetic investigation of methanol synthesis via CO2 hydrogenation on Ni(111)-based surfaces. *Phys. Chem. Chem. Phys.* **2019**, *21*, 20276−20286.
(66) Wang, G.-C.; Nakamura, J. Structure Sensitivity for Forward and Reverse Water-Gas Shift Reactions on Copper Surfaces: A DFT Study. *J. Phys. Chem. Lett.* **2010**, *1*, 3053−3057.
(67) Graciani, J.; Mudiyanselage, K.; Xu, F.; Baber, A. E.; Evans, J.; Senanayake, S. D.; Stacchiola, D. J.; Liu, P.; Hrbek, J.; Sanz, J. F.; Rodriguez, J. A. Highly active copper-ceria and copper-ceria-titania catalysts for methanol synthesis from CO2. *Science* **2014**, *345*, 546−550.
(68) Zhao, Y.-F.; Yang, Y.; Mims, C.; Peden, C. H. F.; Li, J.; Mei, D. Insight into methanol synthesis from CO2 hydrogenation on Cu(111): Complex reaction network and the effects of H2O. *J. Catal.* **2011**, *281*, 199−211.
(69) Cao, K.; Füchsel, G.; Kleyn, A. W.; Juurlink, L. B. F. Hydrogen adsorption and desorption from Cu(111) and Cu(211). *Phys. Chem. Chem. Phys.* **2018**, *20*, 22477−22488.
(70) Frey, K.; Schmidt, D. J.; Wolverton, C.; Schneider, W. F. Implications of coverage-dependent O adsorption for catalytic NO oxidation on the late transition metals. *Catal. Sci. Technol.* **2014**, *4*, 4356−4365.
(71) Fujitani, T.; Nakamura, I.; Uchijima, T.; Nakamura, J. The kinetics and mechanism of methanol synthesis by hydrogenation of CO2 over a Zn-deposited Cu(111) surface. *Surf. Sci.* **1997**, *383*, 285−298.
(72) Jung, K.-D.; Bell, A. T. Role of Hydrogen Spillover in Methanol Synthesis over Cu/ZrO2. *J. Catal.* **2000**, *193*, 207−223.
(73) Fujimoto, K.; Yu, Y. In *New Aspects of Spillover Effect in Catalysis*; Inui, T., Fujimoto, K., Uchijima, T., Masai, M., Eds.; Studies in Surface Science and Catalysis; Elsevier, 1993; Vol. 77; pp 393−396.
(74) Greeley, J.; Mavrikakis, M. Methanol Decomposition on Cu(111): A DFT Study. *J. Catal.* **2002**, *208*, 291−300.
(75) Fu, Q.; Luo, Y. Catalytic Activity of Single Transition-Metal Atom Doped in Cu(111) Surface for Heterogeneous Hydrogenation. *J. Phys. Chem. C* **2013**, *117*, 14618−14624.
(76) Studt, F.; Behrens, M.; Kunkes, E. L.; Thomas, N.; Zander, S.; Tarasov, A.; Schumann, J.; Frei, E.; Varley, J. B.; Abild-Pedersen, F.; Nørskov, J. K.; Schlögl, R. The Mechanism of CO and CO2 Hydrogenation to Methanol over Cu-Based Catalysts. *ChemCatChem* **2015**, *7*, 1105−1111.
(77) Conner, W. C.; Falconer, J. L. Spillover in Heterogeneous Catalysis. *Chem. Rev.* **1995**, *95*, 759−788.
(78) Kim, S. S.; Lee, H. H.; Hong, S. C. The effect of the morphological characteristics of TiO2 supports on the reverse water−gas shift reaction over Pt/TiO2 catalysts. *Appl. Catal., B* **2012**, *119*−*120*, 100−108.
(79) Karelovic, A.; Ruiz, P. The role of copper particle size in low pressure methanol synthesis via CO2 hydrogenation over Cu/ZnO catalysts. *Catal. Sci. Technol.* **2015**, *5*, 869−881.
(80) Wu, H. C.; Chang, Y. C.; Wu, J. H.; Lin, J. H.; Lin, I. K.; Chen, C. S. Methanation of CO2 and reverse water gas shift reactions on Ni/SiO2 catalysts: the influence of particle size on selectivity and reaction pathway. *Catal. Sci. Technol.* **2015**, *5*, 4154−4163.
(81) Kwak, J. H.; Kovarik, L.; Szanyi, J. CO2 Reduction on Supported Ru/Al2O3 Catalysts: Cluster Size Dependence of Product Selectivity. *ACS Catal.* **2013**, *3*, 2449−2455.
(82) Stone, F. S.; Waller, D. Cu−ZnO and Cu−ZnO/Al2O3 Catalysts for the Reverse Water-Gas Shift Reaction. The Effect of the

https://dx.doi.org/10.1021/acscatal.9b05303
ACS Catal. 2020, 10, 4092−4102

Cu/Zn Ratio on Precursor Characteristics and on the Activity of the Derived Catalysts. *Top. Catal.* **2003**, *22*, 305−318.
(83) Karelovic, A.; Galdames, G.; Medina, J. C.; Yévenes, C.; Barra, Y.; Jiménez, R. Mechanism and structure sensitivity of methanol synthesis from CO2 over SiO2-supported Cu nanoparticles. *J. Catal.* **2019**, *369*, 415−426.
(84) Galván, C. Á.; Schumann, J.; Behrens, M.; Fierro, J. L. G.; Schlögl, R.; Frei, E. Reverse water-gas shift reaction at the Cu/ZnO interface: Influence of the Cu/Zn ratio on structure-activity correlations. *Appl. Catal., B* **2016**, *195*, 104−111.
(85) Liu, J.; Shi, J.; He, D.; Zhang, Q.; Wu, X.; Liang, Y.; Zhu, Q. Surface active structure of ultra-fine Cu/ZrO2 catalysts used for the CO2+H2 to methanol reaction. *Appl. Catal., A* **2001**, *218*, 113−119.

https://dx.doi.org/10.1021/acscatal.9b05303
ACS Catal. 2020, 10, 4092−4102